Research Article

Edaravone-loaded poly(amino acid) nanogel inhibits ferroptosis for neuroprotection in cerebral ischemia injury

Yunhan Zhang[a], Zhulin Zou[a], Shuang Liu[a], Fangfang Chen[c], Minglu Li[b], Haoyang Zou[b,], Haiyan Liu[a,*], Jianxun Ding[b]*

[a] *Key Laboratory of Pathobiology Ministry of Education, Department of Anatomy, College of Basic Medical Sciences, Jilin University, Changchun 130061, China*
[b] *Key Laboratory of Polymer Ecomaterials, Changchun Institute of Applied Chemistry, Chinese Academy of Sciences, Changchun 130022, China*
[c] *Department of Gastrointestinal, Colorectal, and Anal Surgery, China-Japan Union Hospital of Jilin University, Changchun 130033, China*

ARTICLE INFO

ABSTRACT

Neurological injury caused by ischemic stroke is a major cause of permanent disability and death. The currently available neuroprotective drugs fail to achieve desired therapeutic efficacy mainly due to short circulation half-life and poor blood–brain barrier (BBB) permeability. For that, an edaravone-loaded pH/glutathione (pH/GSH) dual-responsive poly(amino acid) nanogel (NG/EDA) was developed to improve the neuroprotection of EDA. The nanogel was triggered by acidic and EDA-induced high-level GSH microenvironments, which enabled the selective and sustained release of EDA at the site of ischemic injury. NG/EDA exhibited a uniform sub-spherical morphology with a mean hydrodynamic diameter of 112.3 ± 8.2 nm. NG/EDA efficiently accumulated at the cerebral ischemic injury site of permanent middle cerebral artery occlusion (pMCAO) mice, showing an efficient BBB crossing feature. Notably, NG/EDA with 50 μM EDA significantly increased neuron survival (29.3%) following oxygen and glucose deprivation by inhibiting ferroptosis. In addition, administering NG/EDA for 7 d significantly reduced infarct volume to $22.2\% \pm 7.2\%$ and decreased neurobehavioral scores from 9.0 ± 0.6 to 2.0 ± 0.8. Such a pH/GSH dual-responsive nanoplatform might provide a unique and promising modality for neuroprotection in ischemic stroke and other central nervous system diseases.

* Corresponding authors.
E-mail addresses: hyzou@ciac.ac.cn (H. Zou), haiyan@jlu.edu.cn (H. Liu).
Peer review under responsibility of Shenyang Pharmaceutical University.

1. Introduction

Stroke is one of the most common neurological diseases and the primary cause of disability and death among adults worldwide [1]. Approximately 85% of all stroke cases are categorized as ischemic stroke. It is the leading cause of years of life lost worldwide and often leads to severe, permanent disability, which imposes a heavy burden on public health [2]. Following the blockage of a middle cerebral artery during ischemic stroke, oxygen and glucose depletion in the ischemic core generally induces a secondary oxidative stress response. This response is characterized by the generation of excessive reactive oxygen species (ROS) and inflammatory factors [3], leading to irreversible neuronal death [4].

Thus far, administering thrombus-dissolving drugs, such as tissue plasminogen activator, is the first-line clinical therapy for ischemic stroke [5]. However, due to the narrow time window for administering this treatment, i.e., within 3 − 4.5 h post-onset, only <7% of patients benefit from thrombolytic therapy [1]. Following vessel recanalization, secondary tissue damage caused by ischemia−reperfusion often enlarges the infarct size and worsens the neurological deficit. Approximately 40% of survivors remain disabled after successful recanalization attributed to the secondary reperfusion injury following ischemic stroke [6].

Therefore, neuroprotective agents, such as edaravone (EDA), neurotrophin, and nerve growth factors, offer promise to protect the brain from such overwhelming neurological damage during ischemic stroke. The Japanese Health Authorities approved the small-molecule drug EDA in 2001 to treat ischemic stroke [7]. EDA, a free radical scavenger, has emerged as one of the most commonly used neuroprotective agents for ischemic stroke in clinical practice due to its ability to resist lipid peroxidation and increase the levels of antioxidant enzymes [8,9]. However, the need for frequent and excessive administration due to the short circulation half-life and non-selective release of EDA poses a severe risk of developing toxicity in patients [10]. Thus, it is essential to endow EDA with the ability to target and sustain release while improving its biocompatibility. Recent studies suggested that the nanoparticle-based drug carriers are promising for targeted and selective treatments of ischemic stroke [11,12].

To address the above challenges, an EDA-loaded pH/glutathione (pH/GSH) dual-responsive poly(amino acid) nanogel (NG/EDA) composed of methoxy poly(ethylene glycol)−poly(L-glutamic acid-co-L-cystine) (mPEG−P(Glu-co-Cys^2), NG) was designed and constructed based on acidic pathological characteristic of the ischemic tissue and EDA-induced high-level GSH microenvironments. As depicted in Scheme 1, the designed nanoplatform was constructed to accomplish pH/GSH-triggered EDA release. The in vitro and in vivo results demonstrated that NG/EDA alleviated ischemic brain injury more significantly than free EDA, which is attributed to its better BBB penetration and selective, sustained release behavior of EDA in the ischemic area. NG/EDA ameliorated neurological deficits and secondary damage by inhibiting ferroptosis. This study may provide unique perspectives on the regulatory network between ischemic stroke and ferroptosis and a promising strategy for alleviating cerebral ischemic injury.

2. Materials and methods

2.1. Materials

Methoxy poly(ethylene glycol) (mPEG, number-average molecular weight (M_n) = 2,000 g/mol) was purchased from Sigma-Aldrich (Shanghai, China). The amino-terminated mPEG (mPEG-NH$_2$) was synthesized according to the previously reported literature procedure [13]. γ-Benzyl-L-glutamate and L-cystine were purchased from GL Biochem Co., Ltd. (Shanghai, China). Triphosgene was purchased from Beijing Innochem Science & Technology Co., Ltd. (Beijing, China). Ultra-dry tetrahydrofuran (THF), ultra-dry N,N-dimethylformamide (DMF), trifluoroacetic acid (TFA), and hydrogen bromide solution in acetic acid (33%, 3 ml) were purchased from J&K Scientific Co., Ltd. (Shanghai, China). All the other reagents and solvents were purchased from Sinopharm Chemical Reagent Co., Ltd. (Shanghai, China) and used as obtained. EDA was obtained from MedChemExpress Company (Monmouth Junction, NJ, USA).

Hanks' balanced salt solution (HBSS), Dulbecco's modified Eagle's medium (DMEM), neurobasal medium, glucose-free DMEM, and B27 supplement (50×) were purchased from
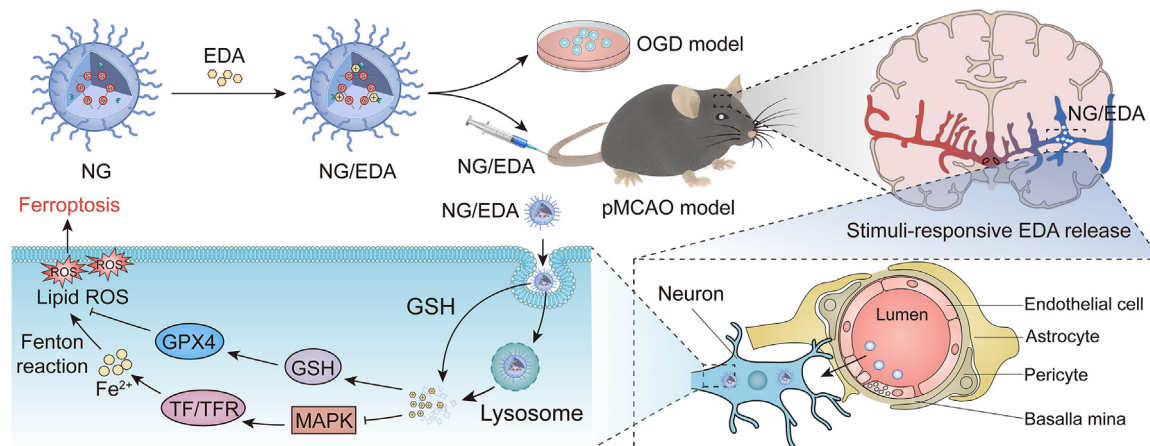
Scheme 1 – Targeted neuroprotection through inhibiting ferroptosis by NG/EDA in cerebral ischemia injury.

Gibco Life Technologies (Grand Island, NY, USA). Fetal equine serum was purchased from Solarbio Life Sciences (Beijing, China). Poly(L-lysine) (PLL, M_n = 150,000−300,000 g/mol), trypsin powder (porcine, 1:250), L-Glutamine, ferrostatin-1 (Fer-1), and erastin were purchased from Sigma-Aldrich Company (St. Louis, MO, USA). Cell counting kit-8 (CCK8) was purchased from Abcam (Cambridge, MA, USA). Iron assay kit was obtained from Sigma-Aldrich (St. Louis, MO, USA). 2′,7′-dichlorofluorescein diacetate (DCFH-DA) probe, GSH, glutathione oxidized (GSSG) assay kit, and malondialdehyde (MDA) assay kit were bought from Beyotime Biotech (Nanjing, China). MitoSOX-Red, BODIPY^{TM} 581/591 C11 (Lipid Peroxidation Sensor phosphatase inhibitor), bicinchoninic acid (BCA) protein assay kit, and enhanced chemiluminescence western blotting substrate were purchased from Thermo Fisher Scientific (Waltham, MA, USA). The relevant information of primary antibodies and secondary antibodies was shown in Table S1. 2,3,5-triphenyl tetrazolium chloride (TTC) was purchased from Sigma-Aldrich (St. Louis, MO, USA).

For an oxygen-glucose deprivation (OGD) model, adult female C57BL/6 pregnant mice purchased from Charles River Laboratories (Beijing, China) were used on the 17th embryonic day. For a permanent middle cerebral artery occlusion (pMCAO) model, 6 to 8 weeks adult male C57BL/6 mice purchased from Charles River Laboratories (Beijing, China) were housed in a specific pathogen-free environment under the condition of 12 h light/12 h dark cycle with free access to food and water, and acclimatized to their surroundings for 3 d. All procedures and treatments were approved by the Ethics Committee of Medical Experiment Animals in the College of Basic Medicine of Jilin University (No. 2019049).

2.2. Preparation of edaravone-loaded poly(amino acid) nanogel

A simple dialysis method loaded EDA into the poly(amino acid) nanogel NG. Briefly, NG (20 mg) was dissolved in 5 ml DMF, and the solution was stirred thoroughly for 12 h. Next, EDA (5 mg) was added, stirring the solution for another 2 h. After that, the solution was slowly added dropwise to 10 ml phosphate-buffered saline (PBS) at pH 7.4 and stirred for 2 h. Subsequently, the solution was transferred to a dialysis bag (molecular weight cutoff (MWCO) = 3,500 Da) and dialyzed with deionized water for 24 h. Finally, the solution was filtered and lyophilized to obtain the NG/EDA. The drug loading content (DLC) and drug loading efficiency (DLE) were calculated according to following equations:

$$DLC\ (\%) = \frac{\text{Weight of EDA in NG/EDA}}{\text{Weight of NG/EDA}} \times 100\%$$

$$DLE\ (\%) = \frac{\text{Weight of EDA in NG/EDA}}{\text{Weight of feeding EDA}} \times 100\%$$

2.3. Edaravone release in vitro

NG/EDA was configured into a 0.1 mg/ml solution and added to a dialysis bag (MWCO = 3,500 Da). The bag was dunked in 100 ml PBS or with 5/10 mM reduced GSH at pH 7.4 or

6.5 and placed in a constant temperature shaker at 37 °C. External buffer (2 ml) was collected and replaced with fresh buffer at 1, 3, 6, 12, 24, 48, and 72 h. The concentration of EDA was determined by high-performance liquid chromatography (HPLC) using a standard curve method which details are described in Supplementary materials.

2.4. Cell viability assay

The survival of primary cultured neurons was assessed using CCK8. The neurons were cultured in 96-well plates precoated with PLL for 10 d. To evaluate cytotoxicity, NG of 0, 10, 50, 100, 200, and 500 µg/ml or NG/EDA with 0, 10, 50, 100, 200, and 500 µM EDA was added to indicated wells containing complete medium, and the cells were incubated at 37 °C with 5% (v/v) CO_2 for 48 h. In addition, neuron cells were treated with NG/EDA (contact with 5, 10, 25, 50, and 100 µM EDA) and Fer-1 (1, 2, 5, 10, 20, 40, and 60 nM) with or without OGD for 4 h. After that, the neurons were treated with different doses of erastin (0, 0.2, 0.5, 5, 10, 20, and 50 µM) with or without NG/EDA (contact with 50 µM EDA) for 24 h in a complete medium at 37 °C with 5% (v/v) CO_2. Next, CCK8 (10 µl) was added to each well, and the cells were incubated for 1−4 h. Finally, the absorbance was read at 450 nm wavelength using a Tecan Austria reader (A-5082, Tecan Trading AG, Männedorf, Switzerland).

2.5. Assessment of intracellular Fe^{2+}

The levels of Fe^{2+} were detected using an iron assay kit according to the instructions provided by the manufacturer. Briefly, the collected neurons (2×10^6 cells) and the cortices of the ischemic territory (10 mg) of mice with pMCAO were homogenized in ice-cold iron assay buffer. The supernatant was obtained after centrifugation at 16,000 g for 10 min to remove insoluble material. For Fe^{2+}, the sample (50 µl) was supplemented with Iron Probe (100 µl) and incubated for 90 min at 25 °C in the dark. Finally, the samples were measured at a wavelength of 593 nm using a Tecan Austria GmbH reader (A-5082). Data were represented as a ratio of the concentration relative to the control/sham (Ctrl/Sham) group.

2.6. Detection of mitochondrial reactive oxygen species

The neurons (5×10^4 cells) were seeded in 24-well plates containing complete medium and incubated at 37 °C with 5% (v/v) CO_2 for 10 d. Subsequently, the cells were incubated with or without EDA (50 µM) or NG/EDA (contact with 50 µM EDA) under OGD for 4 h. Next, a DCFH-DA probe or MitoSOX-Red was added to each well according to the instructions provided by the manufacturer. Images were captured using a ZEISS Imager Z2 confocal microscope (Carl Zeiss AG, Oberkochen, Germany).

2.7. Assessment of lipid peroxidation

Lipid peroxidation was determined with a MDA assay kit, as described by the manufacturer. The collected neurons (2×10^6 cells) and the cortices of the ischemic territory (10 mg) of
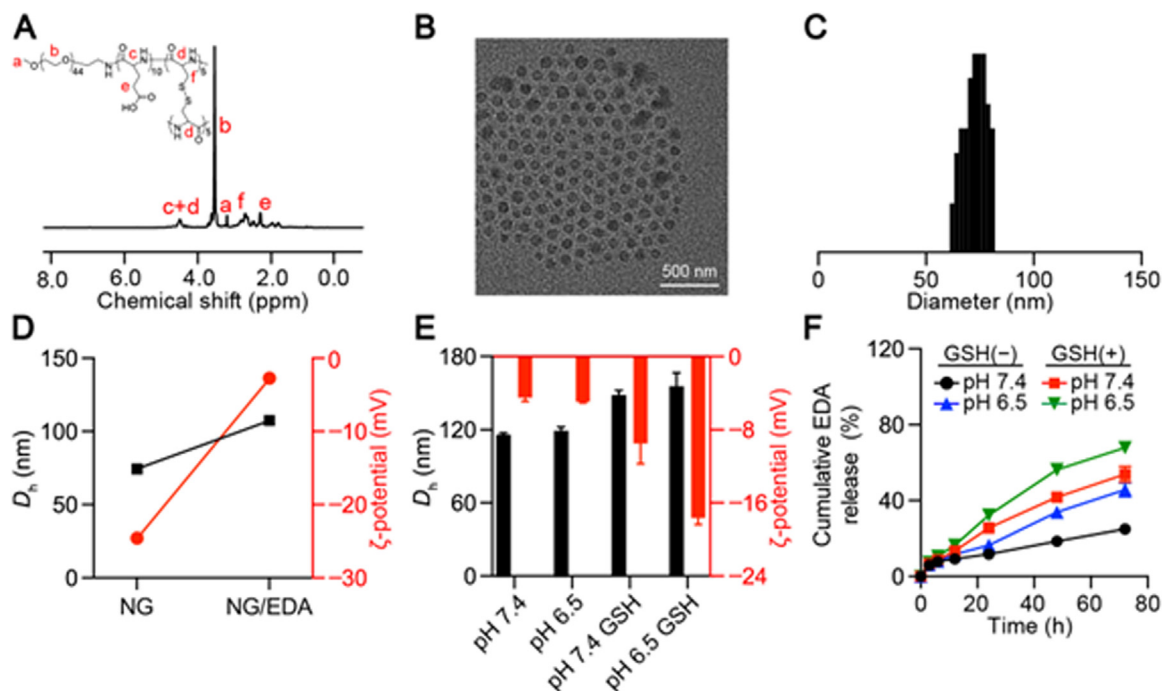
Fig. 1 – Chemical characterizations of NG and NG/EDA: (A) ^{1}H NMR spectrum of NG. (B) Typical TEM image of NG/EDA. (C) Diameter of NG/EDA derived from TEM image. (D) Particle size and ζ-potential changes of NG and NG/EDA. (E) Size and ζ-potential changes of NG/EDA under different conditions for 3 d. (F) EDA release profiles from NG/EDA at pH 6.5 or 7.4 with or without 5 mM GSH. The statistical data are represented as mean ± SD (n = 3).

mice with pMCAO were homogenized in an ice-cold assay buffer. After homogenization, the samples were centrifuged at 10,000 g for 15 min to obtain the supernatant. Following the quantification of protein concentration using a BCA protein assay kit, the supernatant was examined at a wavelength of 530 nm. The MDA levels were expressed as a ratio of concentration to the level of Ctrl/Sham group.

2.8. Assessment of intracellular reduced glutathione

GSH was detected using a GSH and GSSG assay kit according to the instructions provided by the manufacturer. Briefly, the collected neuron cells and the cortices of the ischemic territory (10 mg) of pMCAO mice were added to the protein removal reagent (70 µl). After homogenization, the homogenates were centrifuged at 10,000 g for 10 min at 4 °C, and the supernatant was collected to determine the concentration of total GSH. A GSH-scavenging working solution was added to the supernatant to remove GSH. Finally, samples were analyzed at a wavelength of 530 nm. The levels of GSH were calculated from the total GSH and oxidized GSH measurements and expressed as a ratio of the readings over the concentration recorded in the Ctrl/Sham group.

2.9. Western blotting

After homogenization, the collected primary neurons, cortices of the ischemic territory, and the corresponding tissues of sham-operated mice were lysed in the ice-cold radioimmunoprecipitation assay buffer supplemented with phenylmethylsulfonyl fluoride and phosphatase inhibitors.

The sediment was removed by centrifugation at 12,000 g for 15 min at 4 °C to obtain the supernatant. Protein concentration was determined using a BCA assay kit. After boiling the protein samples in a loading buffer, aliquots (10–15 µg) were loaded in sodium dodecyl sulfate–polyacrylamide gel (8%–15%, w/w) and separated through electrophoresis under constant voltage (100 V). Subsequently, proteins were transferred onto poly(vinylidene fluoride) membranes and incubated with 10% (w/w) skimmed milk powder for 1.5 h. This was followed by incubation with the primary antibody overnight at 4 °C and horseradish peroxidase-linked secondary antibody for 2 h at room temperature. Enhanced chemiluminescence reagent was used for immunodetection and visualization using an Amersham Imager 600 System (General Electric Company, Fairfield, CT, USA).

3. Results and discussion

3.1. Synthesis and characterizations of mPEG−P(Glu-co-Cys^2) with and without edaravone

NG was synthesized through a one-step ring-opening polymerization (ROP) and deprotection strategy, as shown in Scheme S1 [14]. The successful synthesis of NG was confirmed by proton nuclear magnetic resonance (^{1}H NMR) in TFA-d. As shown in Fig. 1A, the signal at 3.5 (b), 2.8 (f), and 2.3 ppm (e) in ^{1}H NMR spectra proved the existence of mPEG, glutamic acid, and cystine, indicating the successful synthesis of NG. Furthermore, the degrees of polymerization (DPs) of glutamic acid and cystine units was 9.8 and 5.1, respectively.

Nanoformulations were produced through the incorporation of EDA into the poly(amino acid) nanoparticle to improve the biocompatibility and selectivity of EDA. The disulfide bond in the cystine unit upregulated the enveloping efficiency of EDA by cross-linking. Moreover, the negative charge generated by the glutamic acid component further enhanced the binding ability with the positively charged EDA based on the positive−negative interaction. In addition, the exposed PEG on the nanogel surface reduced the adsorption of proteins, prolonged circulation time of the nanoformulation, and increased drug accumulation. According to the results obtained through a transmission electron microscope (TEM), NG/EDA was a subspherical particle with a size of 74.3 ± 9.4 nm (Fig. 1B and C). The hydrodynamic diameters (D_hs) of NG and NG/EDA were examined to be 98.2 and 112.3 nm by dynamic laser scattering (DLS) in the intensity model, respectively (Fig. 1D). After loading the EDA, the ζ-potential of NG increased from −19.2 to −2.8 mV, further demonstrating the successful drug loading. Notably, the negative charges prolonged the circulation time of NG/EDA. According to the HPLC result, the DLC and DLE were calculated to be 19.6% and 98.2%, respectively.

To investigate the stability of NG/EDA, we tested the particle size and ζ-potential of NG/EDA under different conditions for 72 h. As shown in Fig. 1E, no significant size change was observed without GSH, indicating that NG/EDA was stable under physiological conditions. However, the particle size of NG/EDA increased remarkably when the conditions of GSH were present. This was mainly due to the breakage of disulfide bonds and the influence of the assembly structure of nanoparticle, increasing the particle size. The change in the ζ-potential of NG/EDA was mainly due to the release of EDA. Under pH 6.5 and GSH conditions, the ζ-potential returned to the level before the loading of EDA, which remained consistent with the release data. It was demonstrated that NG/EDA has good stability under normal physiological conditions.

The pH/GSH dual-responsive nanogel was constructed to achieve sustained and selective drug release from the ischemic brain tissue. The changes in pH affected the positive and negative electrical interactions of EDA and the glutamic acid unit. Furthermore, the disulfide bond in the cystine component could be disrupted by the upregulated level of GSH induced by the EDA at the site of ischemia. This endowed NG/EDA with a pH/GSH dual-responsive property for releasing EDA. The amount of EDA released in PBS with or without GSH at different pH conditions was detected using the dialysis method to examine the drug-release behavior of NG/EDA *in vitro*. The sustained release of EDA was observed over a 72-h period. As shown in Fig. 1F, only < 25% of the EDA was released from NG/EDA in PBS at pH 7.4 within 72 h. It was attributed to the stable coordination between EDA and the glutamic acid component of NG at pH 7.4 and the stability of disulfide bond in the cystine unit of NG in the absence of GSH. During acute ischemia, the pH of the tissue drops to 6.0 − 6.5, at which point NG/EDA rapidly responded to the low pH stimulus to release EDA. This change in the release may be attributed to the protonation of carboxylic group, which weakened NG and EDA coupling. It has been reported

that GSH is present in large amounts in the brain tissue (∼10 mM), while as brain ischemia progresses, GSH drops to ∼5 mM [15]. Several studies have found that EDA significantly reduced the GSH depletion caused by ischemic injury and increased the concentration of GSH [16,17]. When NG/EDA met GSH, the release rate of EDA was significantly increased due to the disruption of the cross-linked structure of NG, which explained the 96.2% release of EDA from NG/EDA within 72 h in a higher GSH concentration of ∼10 mM at pH 6.5 (Fig. S1). Even under lower GSH concentration of ∼5 mM, NG/EDA achieved 67.9% EDA release at 72 h (Fig. 1F). Our data suggested that the increased GSH synergized with low pH to further stimulate the release of EDA from NG/EDA in that case. Thus, these results demonstrated that NG/EDA reduced the EDA release in normal blood circulation and achieved effective, controlled and sustained drug release at the site of ischemic injury.

3.2. Safety evaluation, neuroprotective effect, and mechanism of EDA-loaded nanogel

Neuroprotective therapy is currently the primary treatment strategy to rapidly rescue damaged neurons in the ischemic penumbra [18]. Therefore, we investigated whether NG/EDA protected neurons from ischemic injury. Primary neuron cells were isolated from C57BL/6 mice and subjected to OGD to mimic cerebral ischemic injury *in vitro*. After culture for 10 d, the primary neurons of high purity, 96.4%, as determined by immunofluorescence staining, were obtained (Fig. 2A). CCK8 assay was used to evaluate the survival of neurons subjected to OGD. The results showed that OGD induced death in the neurons in a time-dependent manner (Fig. 2B). Such cell death could be specifically prevented by the use of NG/EDA in a dose-dependent manner at equivalent EDA concentration ranging from 5 to 100 μM (Fig. 2C). Observation by optical microscopy indicated that the neurons in the NG/EDA group maintained a complete neural network, and the number of axons in the same field was higher in this group compared with that in the EDA group (Fig. 2D and E). Consequently, NG/EDA possessed markedly higher neuroprotective activity *versus* the free drug EDA. HPLC was used to detect the level of EDA in neuronal cells after incubation of free EDA or NG/EDA for 6 h. The data showed that the intracellular concentration of EDA was significantly higher in the NG/EDA group, suggesting that NG/EDA had better cell uptake ability than free EDA (Fig. S2). We subsequently evaluated the safety of NG/EDA. After incubation with increasing concentration of NG or NG/EDA for 48 h, the neurons maintained high rates of cell viability at 93.1% or 95.7%, respectively. These findings demonstrated the satisfactory biosafety of NG/EDA (Fig. S3 and S4). Therefore, developing a nanoformulation for EDA is a safe and effective strategy.

Ferroptosis is a newly recognized type of cell death driven by iron-dependent lipid peroxidation [19]. It was recently confirmed that ferroptosis was involved in neurological impairment after cerebral ischemia [20]. Hence, we further investigated whether ferroptosis played a crucial regulatory role in stroke. We recorded the following observations to support the hypothesis that NG/EDA protected the neurons from an ischemic stroke *via* ferroptosis:
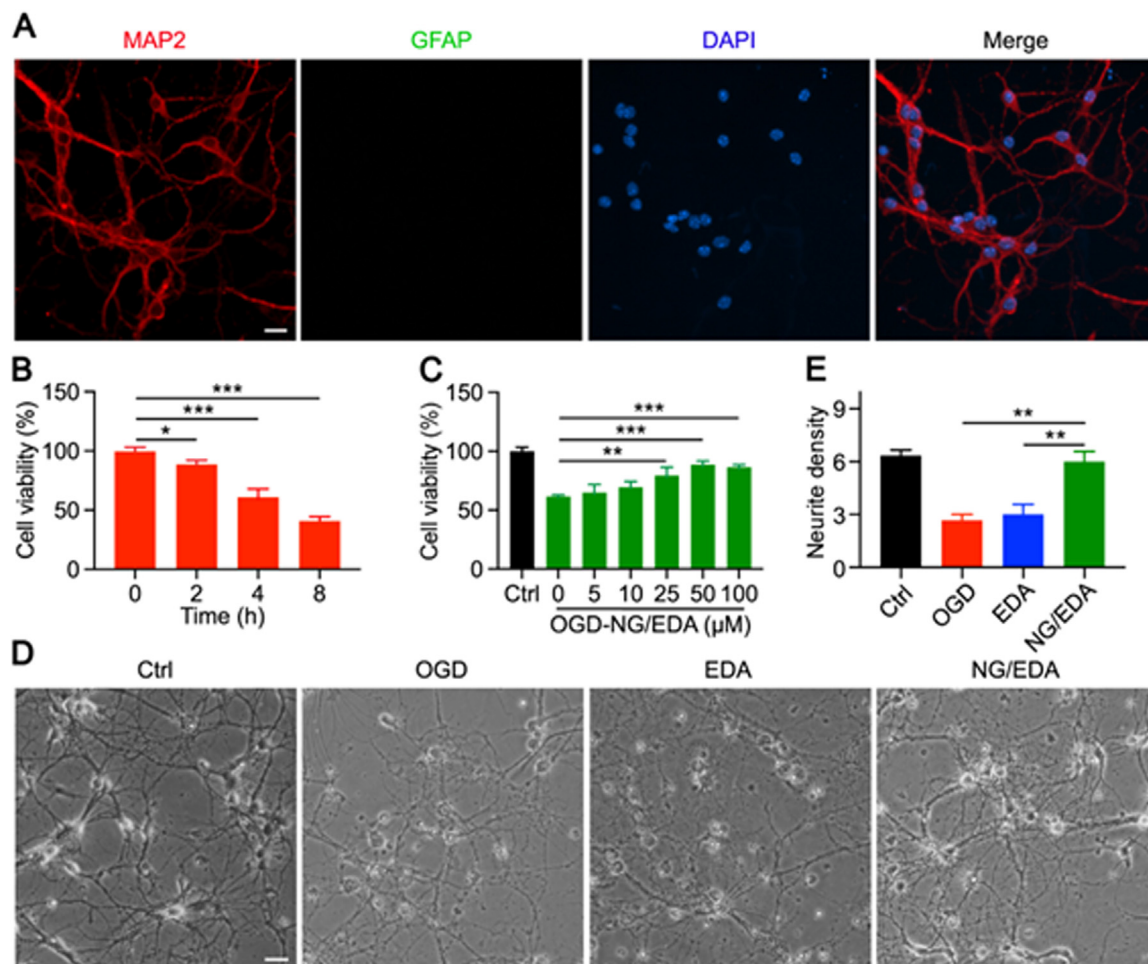
Fig. 2 – NG/EDA alleviated injury in the neurons subjected to OGD. (A) The primary cultured neurons were stained using the neuron marker microtubule-associated protein 2 (MAP2) and the astrocyte marker glial fibrillary acidic protein (GFAP) to confirm their purity (scale bar: 20.0 μm). (B) Cell viability of the neurons subjected to OGD was evaluated using the CCK8 assay. (C) Following OGD, the neurons were treated with increasing concentrations of NG/EDA containing 0, 5, 10, 25, 50, and 100 μM EDA. (D) Microscopic morphologies of neurons (scale bar: 20.0 μm). (E) Quantification of neurite numbers was analyzed using ImageJ software. The statistical data are represented as mean ± SD ($n = 3$; *$P < 0.05$, **$P < 0.01$, ***$P < 0.001$).

(1) Although ferroptosis could be triggered *via* different pathways, it was commonly inhibited by ferroptosis antagonists, such as Fer-1 [21]. Pretreatment with Fer-1 reversed the death of neurons subjected to OGD, and NG/EDA with 50 μM EDA significantly rescued the neuronal injury induced by ferroptosis inducer erastin (Fig. 3A−3C). These results illustrated that ferroptosis was caused by OGD, while NG/EDA reversed the erastin-induced ferroptosis. Therefore, we suggested that NG/EDA inhibited ferroptosis.

(2) Iron overload was considered a typical feature of ferroptosis [22]. The level of Fe^{2+} was determined using an iron assay kit. We found that NG/EDA with 50 μM EDA significantly decreased the relative Fe^{2+} levels (*i.e., versus* those recorded in the Ctrl group) from 1.9 to 0.9 in the model of neurons subjected to OGD. In contrast, the effect of EDA on Fe^{2+} levels was limited (Fig. 3D).

(3) ROS was a crucial target for preventing ferroptosis [23]. Intracellular ROS levels were measured using a DCFH-DA probe. OGD induced a significant increase in the levels of ROS. In contrast, weak green fluorescence was observed in the Ctrl and NG/EDA groups (Fig. 3E).

(4) Mitochondrial dysfunction induced by increased mitochondrial ROS was critical for ferroptosis [24]. Mitochondrial superoxide indicator MitoSOX Red was used to detect mitochondrial ROS. Fluorescence analysis revealed that NG/EDA markedly neutralized the OGD-mediated increase of mitochondrial ROS, whereas EDA failed to exert such an effect (Fig. 3F).

(5) MDA, the final product of the peroxidation of polyunsaturated fatty acids, was overproduced during ferroptosis [25]. As shown in Fig. 3G, the intracellular MDA level was significantly lower in the neurons treated with NG/EDA than in those subjected to OGD or treated with EDA. A lipid peroxidation sensor, BODIPY 581/591
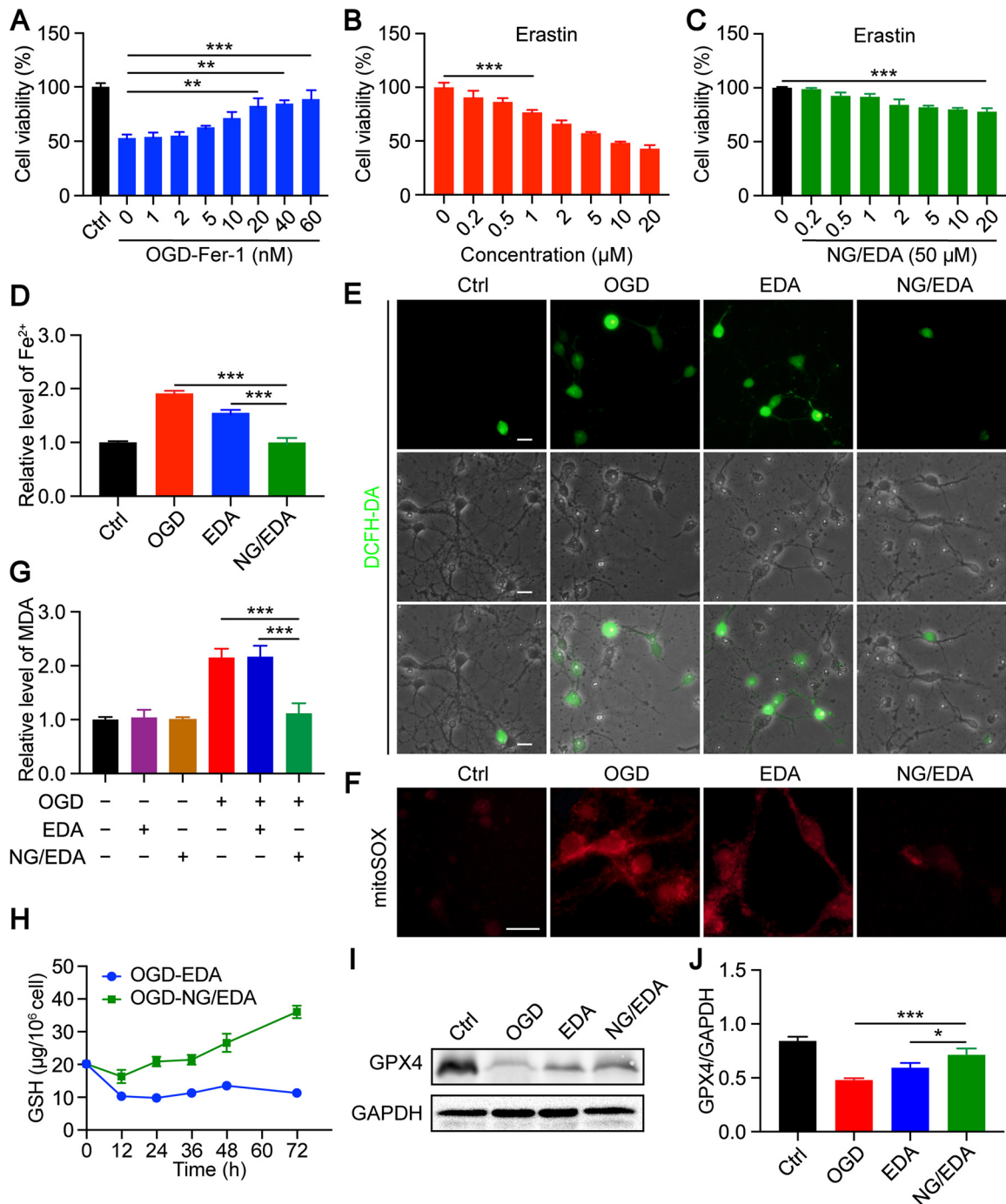
Fig. 3 – NG/EDA attenuated the insult induced by OGD through inhibiting ferroptosis. (A) Cell viability after treatment with Fer-1 to overcome OGD-induced neuronal injury. **(B)** Cell viability after treatment with erastin for 24 h. **(C)** Cell viability after treatment with increasing dose of erastin and NG/EDA for 24 h. **(D)** Iron assay was used to detect changes in the concentration of intracellular Fe^{2+} in the primary neurons. **(E)** Analysis of ROS levels inside neurons (scale bar: 20.0 μm). **(F)** Representative MitoSOX Red images of mitochondrial ROS in damaged neurons (scale bar: 20.0 μm). **(G)** The production of lipid peroxidation was measured using the MDA assay. **(H)** Time-dependent profile of GSH content under OGD condition. **(I)** Western blotting analysis of protein expression of GPX4. **(J)** Quantification of immunoblotted protein in extracts from primary cultured neurons. The statistical data are represented as mean ± SD ($n = 3$; *$P < 0.05$, **$P < 0.01$, ***$P < 0.001$).
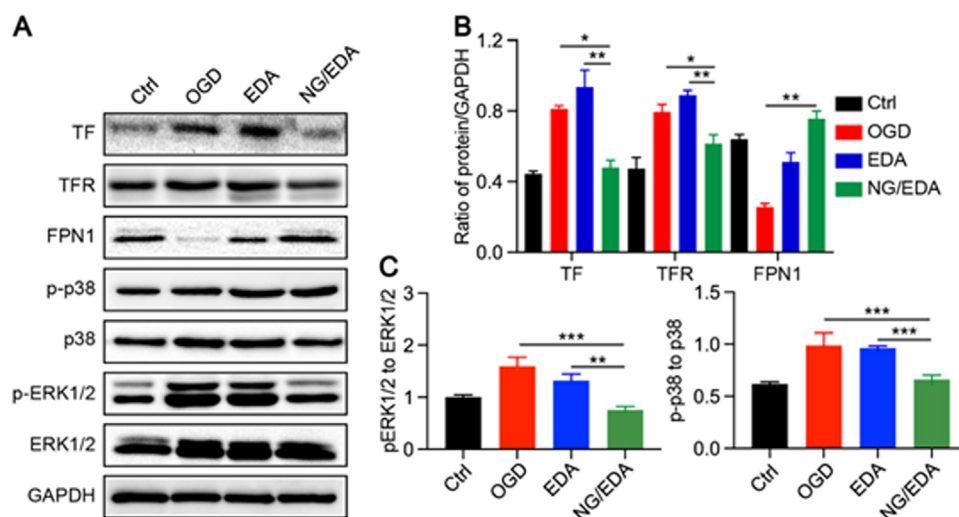
Fig. 4 – Effect of NG/EDA on iron metabolism in neurons subjected to OGD. (A) Western blotting was used to analyze the levels of proteins related to ferroptosis and the p38/ERK MAPK pathway in cells after treatment. (B,C) Quantification analysis for TF, TFR, FPN1, p-p38, p38, p-ERK1/2, and ERK1/2. The statistical data are represented as mean ± SD ($n = 3$; *$P < 0.05$, **$P < 0.01$, ***$P < 0.001$).

C11, was used to label the OGD neurons, and the results showed that NG/EDA decreased the final products of lipid peroxidation induced by OGD damage (Fig. S5). These observations indicated that the inhibition of ferroptosis by NG/EDA was attributed to the efficient removal of excessive lipid peroxide in injured cells.

(6) Depletion of endogenous antioxidant enzymes, *i.e.*, GSH and glutathione peroxidase 4 (GPX4), was considered the leading cause of neuronal susceptibility to ferroptosis [26]. GSH analysis showed that EDA mitigated the depletion of GSH induced by OGD; however, the effect was significantly less pronounced than that recorded in the NG/EDA group (Fig. S6). These changes indicated that NG/EDA inhibited ferroptosis by activating the antioxidant enzymes. Furthermore, we found that differences in the GPX4 enzyme in neuron models were consistent with those noted for GSH (Fig. 3I and J).

GSH analysis also found that the content of GSH in the neurons treated with EDA or NG/EDA decreased to varying degrees when OGD stimulation lasted to 12 h, which was attributed to the severe consumption of GSH induced by continuous glucose and oxygen depletion. NG/EDA significantly increased GSH level under OGD within 24 h. When the stimulation lasted for 72 h, the GSH content of NG/EDA group was significantly higher than that of the EDA group, which was 1.89 times that of the Ctrl group (Fig. 3H). There is evidence that under OGD condition, glycolysis was enhanced in the primary neurons, leading to ambient acidification [27]. The results suggest that NG/EDA rapidly released EDA in response to low pH stimulation in the early stage of OGD. The initial release of EDA increases the GSH level of damaged neurons and further promotes residual EDA release in NG/EDA. This analysis further explained that NG/EDA was superior to free EDA in cell uptake, as mentioned above (Fig. S2).

Our observations showed that NG/EDA effectively inhibited the OGD-mediated ferroptosis and the synergistic effect of pH/GSH dual-responsiveness might be beneficial to the cell uptake of NG/EDA and the sustained release of EDA.

A recent study demonstrated that the mitogen-activated protein kinase (MAPK) signaling pathway plays a causative role in mediating ferroptosis through the regulation of iron metabolism [28]. The activation of p38/extracellular regulated kinase (p38/ERK) MAPK pathway upregulated the expression of transferrin (TF) and transferrin receptor (TFR) after ischemic stroke, which acted as central regulators to transport extracellular Fe^{3+} into the cells. Ferroportin 1 (FPN1) was the only known efflux pump for iron ions [29]. The expression of TF, TFR and FPN1 in the primary cultured neurons following treatment was detected to clarify whether the abnormal changes in the intracellular Fe^{2+} were associated with the MAPK-mediated upregulation of Fe^{2+}/Fe^{3+} transport-related proteins. An obvious upregulation of TF and TFR was observed after OGD-induced injury, whereas the expression of FPN1 was significantly decreased. These data suggested that the Fe^{3+} influx mediated by TF and TFR was increased, whereas the Fe^{2+} efflux mediated by FPN1 was inhibited after glycogen depletion. Subsequently, we found that the phosphorylation levels of p38 and ERK1 and 2 (ERK1/2) (*i.e.*, the ratio of phosphorylated protein levels over the total protein levels) were significantly increased after OGD-induced injury, indicating the activation of p38/ERK MAPK pathway. Of note, both EDA and NG/EDA decreased the abnormal elevation in the expression of phosphorylated-ERK1/2 (p-ERK1/2) and phosphorylated-p38 (p-p38) to a certain extent. This was accompanied by a corresponding decrease in the TF and TFR expression. However, the inhibitory effect of NG/EDA was more significant than that of EDA (Fig. 4A−4C). These changes in the expression of key proteins suggested that NG/EDA significantly inhibited the activation of p38/ERK pathway to reduce the influx of exogenous Fe^{2+} by regulating the above iron metabolism-related proteins. This evidence
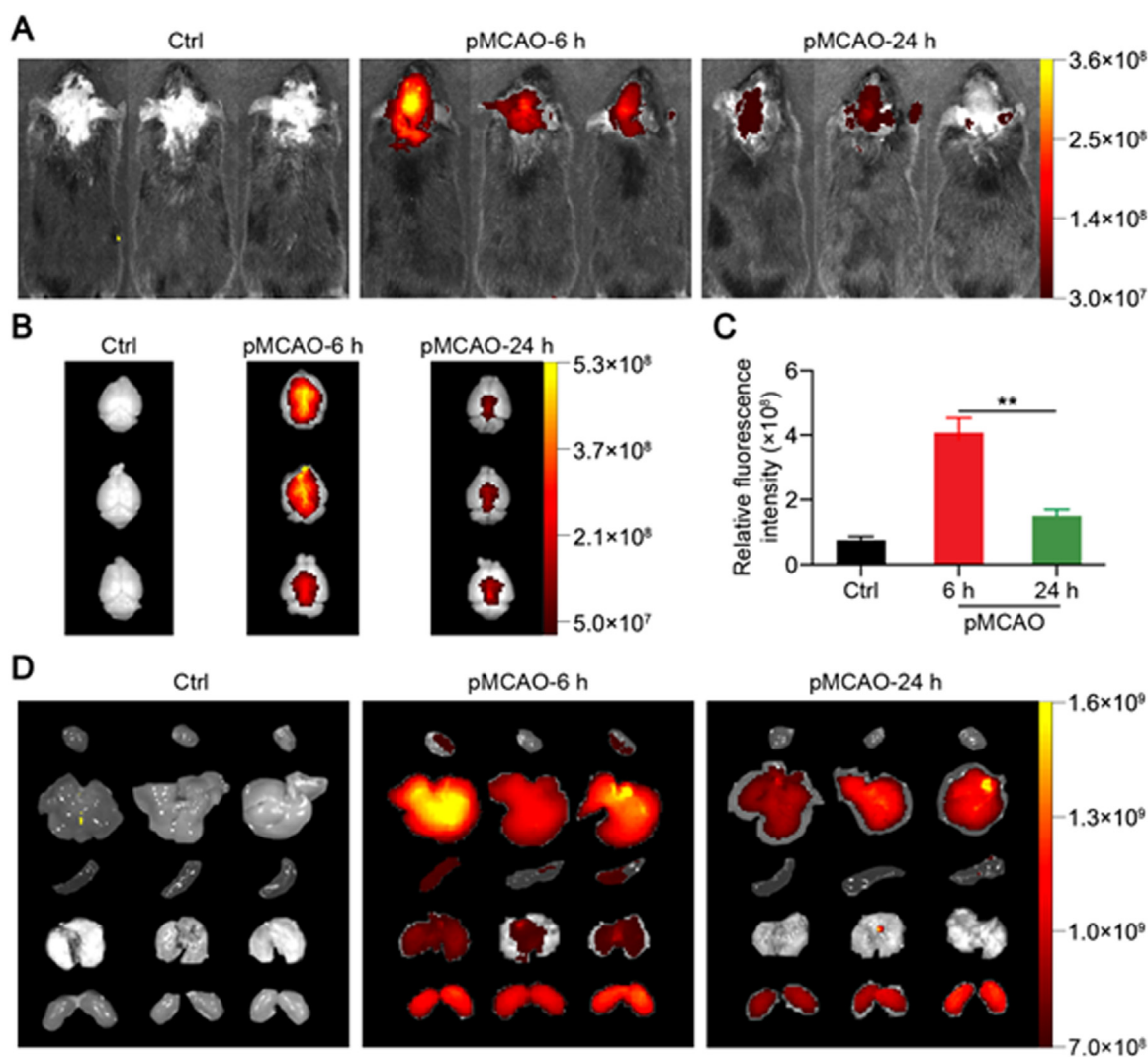
Fig. 5 – Biodistribution of NG/EDA in pMCAO mouse model. (A) *In vivo* **fluorescence imaging of pMCAO mice of 6 h after i.v. injection of PBS at 6 or 24 h after i.v. injection of Cy5.5-NG/EDA. (B)** *Ex vivo* **fluorescence imaging of brains collected from pMCAO mice at 6 h after i.v. injection of PBS and 6 or 24 h after i.v. injection of Cy5.5-NG/EDA. (C) The fluorescence intensity of brains in (B) was quantified by ImageJ software. (D)** *Ex vivo* **fluorescence imaging of hearts, livers, spleens, lungs, and kidneys from pMCAO mice at 6 h after i.v. injection of PBS and at 6 or 24 h after i.v. injection of Cy5.5-NG/EDA. The statistical data are represented as mean ± SD (*n* = 3; *P < 0.05).**

explained the inhibitory effect of NG/EDA on OGD-induced ferroptosis in terms of iron metabolism.

However, the regulatory network underlying the interaction between iron metabolism-related proteins and the p38/ERK MAPK signaling pathway was not fully understood. Hence, further investigation was warranted to determine how the pathway regulates iron metabolism.

3.3. *Neuroprotective effect of EDA-loaded nanogel in permanent middle cerebral artery occlusion mice*

To evaluate the biodistribution and *in vivo* targeting of NG/EDA, NG/EDA was labeled with Cy5.5 (Cy5.5-NG/EDA) and intravenously (*i.v.*) injected into pMCAO mice to observe the distribution *in vivo*. Six hours after *i.v.* injection of Cy5.5-NG/EDA, the fluorescent signal in the brain was strong (Fig. 5A). This result was consistent with previous reviews that

nanoparticles at about 100 nm are ideal for penetrating the BBB [30]. Similarly, *ex vivo* imaging results showed that the fluorescence signal in the whole brain of pMCAO mice was significantly enhanced at 6 h and decreased to 44.8% after 24 h (Fig. 5B and C). In addition, NG/EDA was mainly accumulated in the liver and kidney. The fluorescence intensity in the liver and kidney maintained high prior to 6 h, while it decreased at 24 h after *i.v.* injection (Fig. 5D). Accordingly, we determined the dosing interval to be every 24 h in subsequent *in vivo* experiments.

We subsequently conducted an *in vivo* evaluation of the neuroprotective performance of NG/EDA in the mice with pMCAO. The design and timeline of experiments performed using the mouse model of pMCAO are shown in Fig. 6A. The neurological severity score (NSS) was lower in the NG/EDA-3 d group (5.2 ± 0.9) compared with those in the saline-3 d (9.0 ± 0.6) and EDA-3 d (7.8 ± 0.7) groups
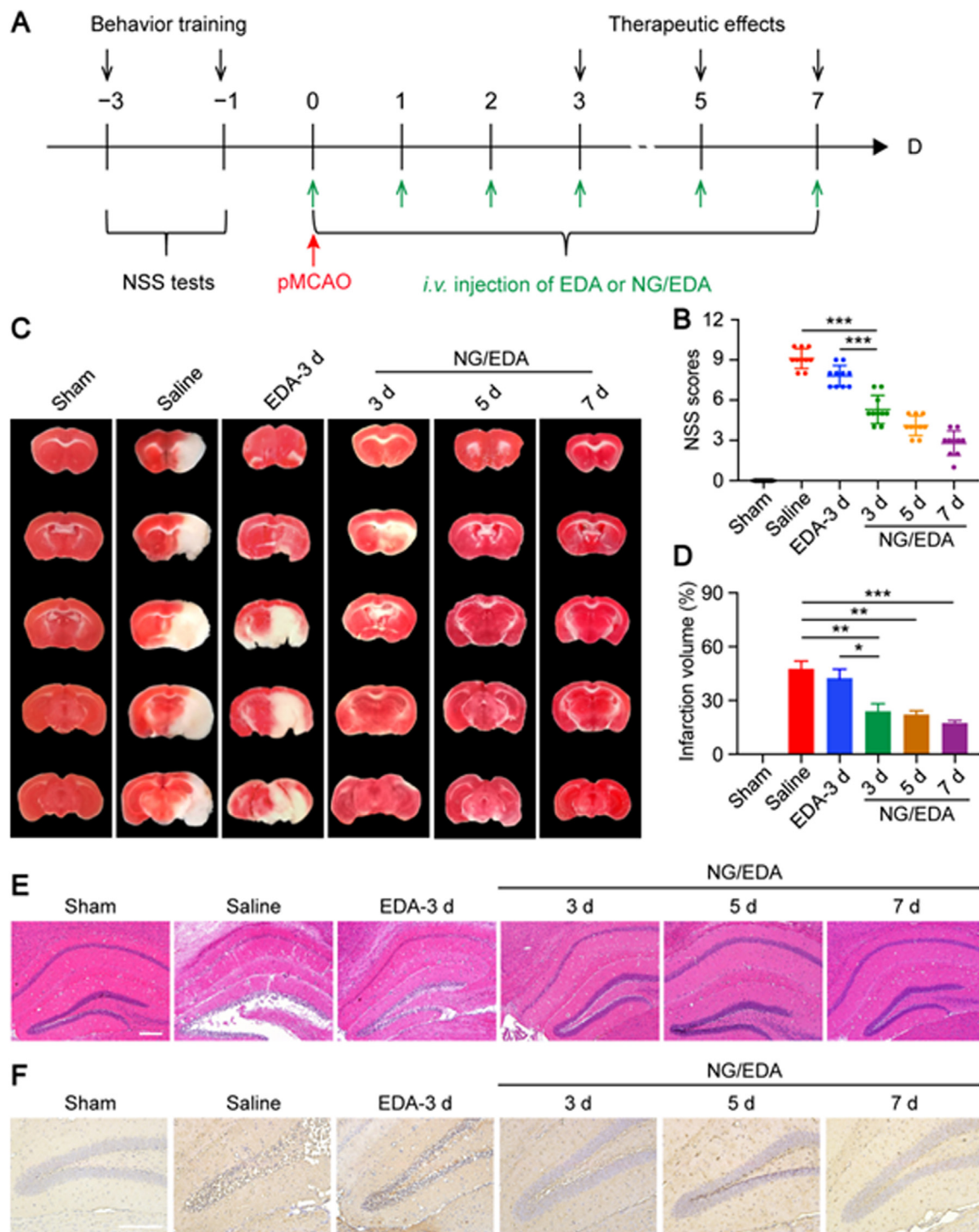
Fig. 6 – NG/EDA alleviated cerebral ischemic injury in the mice with pMCAO. (A) Timeline and design of animal experiments. (B) NSS data in mice with pMCAO after treatments with saline or EDA for 3 d and NG/EDA for 3, 5 or 7 d ($n = 10$). (C) Representative images of TTC staining in coronal brain slides and (D) quantitative analysis of infarct volume ($n = 5$) using ImageJ software. (E) H&E staining of neurons in hippocampal CA1 region of mice with pMCAO after aforementioned treatments (scale bar: 100.0 μm). (F) IHC staining of neurons in hippocampal DG region of mice with pMCAO after the aforementioned treatments (scale bar: 100.0 μm). The statistical data are represented as mean ± SD (**$P < 0.01$, ***$P < 0.001$).
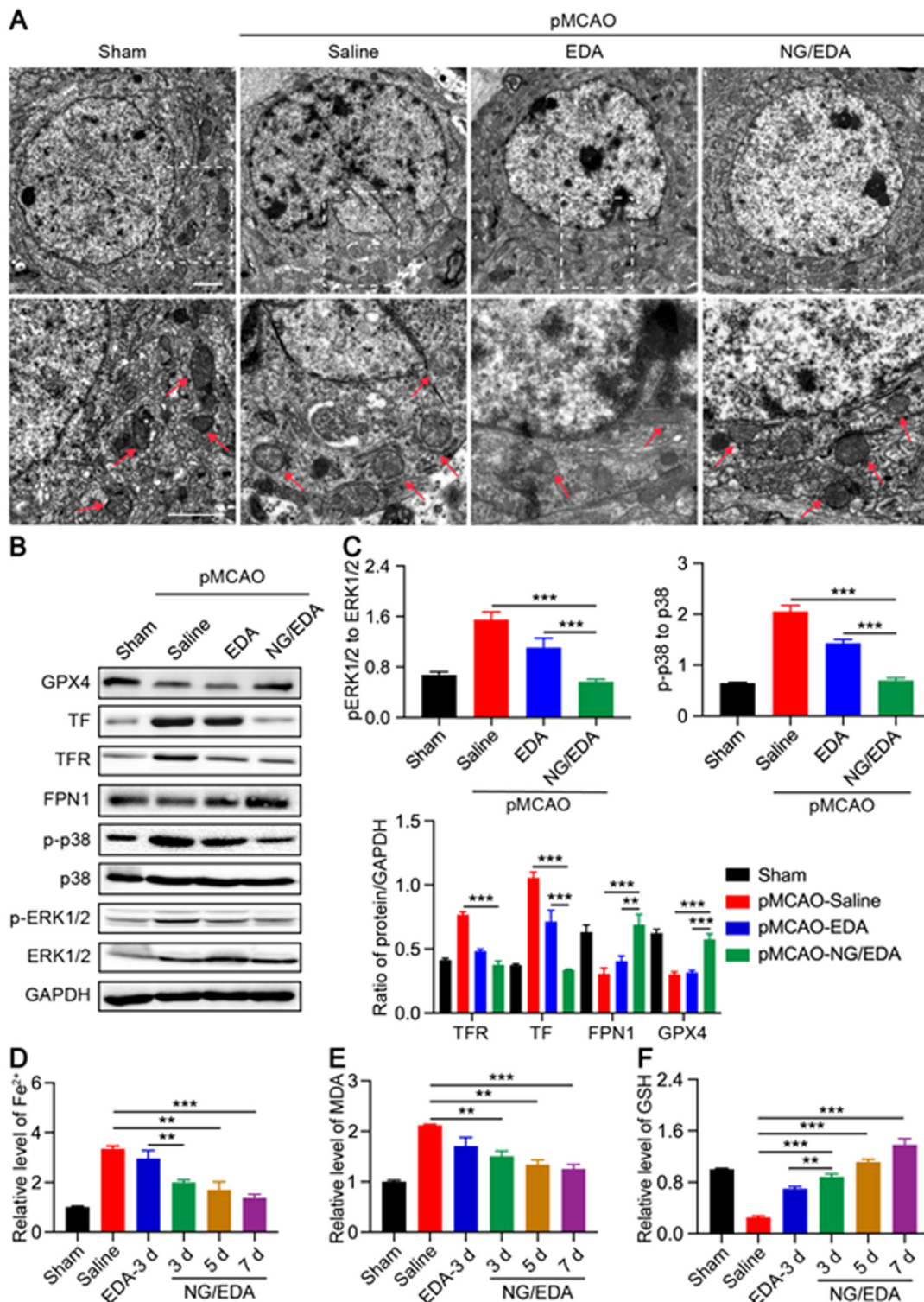
Fig. 7 – NG/EDA inhibited the p38/ERK MAPK pathway involved in ferroptosis induced by cerebral ischemic injury. (A) TEM was used to observe the morphologies of neurons in a mouse model of pMCAO (scale bar: 1.0 µm). (B) Western blotting was used to assess the protein levels in the cerebral extracts obtained from mice. (C) Quantitative analysis of expression of GPX4, TF, TFR, FPN1, p-p38, p38, p-ERK1/2 and ERK1/2. (D−F) Assessment of intracellular Fe^{2+}, MDA and GSH levels in the mouse brain after indicated treatments. The statistical data are represented as mean ± SD ($n = 3$; *$P < 0.05$, **$P < 0.01$, ***$P < 0.001$).

(Fig. 6B). The evaluation of the inhibitory effect of NG/EDA on ferroptosis was extended to 7 d after pMCAO, which still showed more efficient neuroprotection than free EDA. The infarct volume was evaluated through TTC staining. Consistent with the above results, the NG/EDA-3 d group exhibited a more significant reduction in infarct volume compared with the EDA-3 d group. These findings indicated that NG/EDA exerted better neuroprotection than EDA at a dose of 2.0 mg/(kg BW) (Fig. 6C and D). Importantly, these changes became more pronounced following the prolongation of treatment with NG/EDA to 5 or 7 d, which suggested that NG/EDA gradually attenuated severe neurological dysfunction in the mice with pMCAO in a time-dependent manner. Consistent with these observations, NG/EDA exerted an obvious protective effect on the hippocampal neurons in the CA1 region, the major region of neuronal injury, as demonstrated by hematoxylin and eosin (H&E) staining (Fig. 6E and S7). S100b existed specifically in central nerve cells; overexpression of S100b indicated insults to the neurons [31]. Hence, the expression of S100b was assessed after the ischemic stroke. Immunohistochemistry (IHC) images substantiated that NG/EDA reversed the overexpression of S100b in the hippocampal dentate gyrus neurons subjected to pMCAO (Fig. 6F and S8). These results suggested that the selective release of EDA from NG/EDA exerted a targeted neuroprotective effect in the damaged hemisphere.

NG/EDA was able to protect the primary neurons against neurological damage through the inhibition of ferroptosis. Thus, we investigated whether NG/EDA protected the neurons and antagonized ferroptosis in permanent ischemia *in vivo*. Morphologically, ferroptosis cells exhibit ultrastructural changes in mitochondria [32]. The absence of apoptotic bodies or autophagosomes in ferroptosis cells and the absence of swelling of organelles or rupture of cell membranes were striking features distinguishing ferroptosis from other forms of cell death [33]. The morphology of neurons in the sham, saline, EDA, and NG/EDA groups was examined through TEM. Compared with those in the saline and EDA groups, neurons in the sham and NG/EDA groups exhibited an intact cell membrane and a linear or granular appearance of mitochondria with an intact double-layered membrane structure. In the saline and EDA groups, the images showed that mitochondria shrank, the inner mitochondrial cristae decreased or disappeared, and the outer mitochondrial membrane was damaged (Fig. 7A). This evidence illustrated that NG/EDA significantly inhibited the neuronal ferroptosis induced by an ischemic hypoxic insult. The protein analysis corroborated these findings. The results revealed significant increases in the TF and TFR levels and reductions in the FPN1 and GPX4 levels in the ipsilateral damaged hemisphere after pMCAO. Nevertheless, NG/EDA attenuated the abnormal expression of above proteins (Fig. 7B and C). We also analyzed the expression of related proteins to provide evidence that the NG/EDA-mediated change in the p38/ERK MAPK pathway in response to ischemic insult-induced ferroptosis *in vivo*. The results were similar to those obtained *in vitro*; increased phosphorylation of ERK1/2 and p38 was observed in the ischemic insult group. NG/EDA reversed the protein concentration to basal levels, indicating successful inhibition of the p38/ERK MAPK pathway. Consistent with the above

results in the model of OGD, NG/EDA significantly inhibited ferroptosis. This was reflected by the gradual reversal of elevation in the Fe^{2+} level (Fig. 7D), the increase in one of the final products of lipid peroxidation MDA (Fig. 7E), or the membrane intensity of lipid peroxidation sensor BODIPY 581/591 C11 (Fig. S9), and the depletion of GSH (Fig. 7F). This result had also led to the discovery that NG/EDA partially released EDA in response to dropped pH in the ischemic area at the initial stage. With the significant increase in the GSH level, the synergistic effect of pH/GSH dual-responsiveness further improved the local release of EDA.

The present results suggested that NG/EDA achieved selective and sustained drug release in the injured ischemic hemisphere and exerted long-term neuroprotection against ischemic stroke by inhibiting ferroptosis.

4. Conclusion

This study developed a pH/GSH dual-responsive poly(amino acid) nanogel as a delivery vehicle of EDA to achieve targeted molecular therapy for ischemic stroke. They were demonstrated to effectively deliver EDA across the BBB and enable sustained and selective release in the ischemic area site. Moreover, NG/EDA exerted neuroprotective effects *via* inhibiting ferroptosis, thus alleviating neurological deficits and reversing ischemic insults. It protected the damaged primary neurons and ischemic mice from ferroptosis by regulating the MAPK signal pathway *via* iron metabolism-related proteins, increasing antioxidant enzyme levels, and reducing lipid peroxide accumulation. In conclusion, the NG/EDA-derived nanotherapies might become a valuable clinical option for treating ischemic stroke and other central nervous system diseases.

Declaration of Competing Interest

The authors declare that they have no known competing financial interests or personal relationships that could have appeared to influence the work reported in this paper.

Acknowledgements

Supplementary materials

Supplementary material associated with this article can be found, in the online version, at doi:10.1016/j.ajps.2024.100886.

References

[1] Donnan GA, Davis SM, Parsons MW, Ma H, Dewey HM, Howells DW. How to make better use of thrombolytic therapy in acute ischemic stroke. Nat Rev Neurol 2011;7(7):400–9.

[2] Roth GA, Abate D, Abate KH, Abay SM, Abbafati C, Abbasi N, et al. Global, regional, and national age-sex-specific mortality for 282 causes of death in 195 countries and territories, 1980–2017: a systematic analysis for the Global Burden of Disease Study 2017. Lancet 2018;392(10159):1736–88.

[3] Lakhan SE, Kirchgessner A, Hofer M. Inflammatory mechanisms in ischemic stroke: therapeutic approaches. J Translational Med 2009;7(1):1–11.

[4] Yuan J, Li L, Yang Q, Ran H, Wang J, Hu K, et al. Targeted treatment of ischemic stroke by bioactive nanoparticle-derived reactive oxygen species responsive and inflammation-resolving nanotherapies. ACS Nano 2021;15(10):16076–94.

[5] Gauberti M, Martinez de Lizarrondo S, Vivien D. Thrombolytic strategies for ischemic stroke in the thrombectomy era. J Thromb Haemost 2021;19(7):1618–28.

[6] Zhang SR, Phan TG, Sobey CG. Targeting the immune system for ischemic stroke. Trends Pharmacol Sci 2021;42(2):96–105.

[7] Kikuchi K, Tanaka E, Murai Y, Tancharoen S. Clinical trials in acute ischemic stroke. CNS Drugs 2014;28:929–38.

[8] Noor JI, Ikeda T, Ueda Y, Ikenoue T. A free radical scavenger, edaravone, inhibits lipid peroxidation and the production of nitric oxide in hypoxic-ischemic brain damage of neonatal rats. Am J Obstet Gynecol 2005;193(5):1703–8.

[9] Watanabe T, Tahara M, Todo S. The novel antioxidant edaravone: from bench to bedside. Cardiovasc Ther 2008;26(2):101–14.

[10] Jin Q, Cai Y, Li S, Liu H, Zhou X, Lu C, et al. Edaravone-encapsulated agonistic micelles rescue ischemic brain tissue by tuning blood-brain barrier permeability. Theranostics 2017;7(4):884.

[11] Du Y, Huo Y, Yang Q, Han Z, Hou L, Cui B, et al. Ultrasmall iron-gallic acid coordination polymer nanodots with antioxidative neuroprotection for PET/MR imaging-guided ischemia stroke therapy. Exploration 2023;3(1):20220041.

[12] Yang Q, Pu W, Hu K, Hu Y, Feng Z, Cai J, et al. Reactive oxygen species-responsive transformable and triple-targeting butylphthalide nanotherapy for precision treatment of ischemic stroke by normalizing the pathological microenvironment. ACS Nano 2023;17(5):4813–33.

[13] Thompson MS, Vadala TP, Vadala ML, Lin Y, Riffle JS. Synthesis and applications of heterobifunctional poly(ethylene oxide) oligomers. Polymer 2008;49(2):345–73.

[14] Xing T, Lai B, Ye X, Yan L. Disulfide core cross-linked PEGylated polypeptide nanogel prepared by a one-step ring opening copolymerization of N-carboxyanhydrides for drug delivery. Macromol Biosci 2011;11(7):962–9.

[15] Wallin C, Puka-Sundvall M, Hagberg H, Weber SG, Sandberg M. Alterations in glutathione and amino acid concentrations after hypoxia–ischemia in the immature rat brain. Dev Brain Res 2000;125(1–2):51–60.

[16] Liu L, Song Y, Zhao M, Yi Z, Zeng Q. Protective effects of edaravone, a free radical scavenger, on lipopolysaccharide-induced acute kidney injury in a rat model of sepsis. Int Urol Nephrol 2015;47:1745–52.

[17] Dang R, Wang M, Li X, Wang H, Liu L, Wu Q, et al. Edaravone ameliorates depressive and anxiety-like behaviors via Sirt1/Nrf2/HO-1/Gpx4 pathway. J Neuroinfla 2022;19(1):1–29.

[18] Baron JC. Protecting the ischaemic penumbra as an adjunct to thrombectomy for acute stroke. Nat Rev Neurol 2018;14(6):325–37.

[19] Yang WS, Stockwell BR. Ferroptosis: death by lipid peroxidation. Trends Cell Biol 2016;26(3):165–76.

[20] She X, Lan B, Tian H, Tang B. Cross talk between ferroptosis and cerebral ischemia. Front Neurosci 2020;14:776.

[21] Shah R, Shchepinov MS, Pratt DA. Resolving the role of lipoxygenases in the initiation and execution of ferroptosis. ACS Cent Sci 2018;4(3):387–96.

[22] Dixon SJ, Stockwell BR. The role of iron and reactive oxygen species in cell death. Nat Chem Biol 2014;10(1):9–17.

[23] Gao M, Monian P, Pan Q, Zhang W, Xiang J, Jiang X. Ferroptosis is an autophagic cell death process. Cell Res 2016;26(9):1021–32.

[24] Angelova PR, Esteras N, Abramov AY. Mitochondria and lipid peroxidation in the mechanism of neurodegeneration: finding ways for prevention. Med Res Rev 2021;41(2):770–84.

[25] Gaschler MM, Stockwell BR. Lipid peroxidation in cell death. Biochem Biophys Res Commun 2017;482(3):419–25.

[26] Seibt TM, Proneth B, Conrad M. Role of GPX4 in ferroptosis and its pharmacological implication. Free Radic Biol Med 2019;133:144–52.

[27] Li Z, Zhang B, Yao W, Zhang C, Wan L, Zhang Y. APC-Cdh1 regulates neuronal apoptosis through modulating glycolysis and pentose-phosphate pathway after oxygen-glucose deprivation and reperfusion. Cell Mol Neurobiol 2019;39:123–35.

[28] Wang X, Tan X, Zhang J, Wu J, Shi H. The emerging roles of MAPK-AMPK in ferroptosis regulatory network. Cell Commun Signal 2023;21(1):200.

[29] Song Q, Peng S, Che F, Zhu X. Artesunate induces ferroptosis via modulation of p38 and ERK signaling pathway in glioblastoma cells. J Pharmacol Sci 2022;148(3):300–6.

[30] Terstappen GC, Meyer AH, Bell RD, Zhang W. Strategies for delivering therapeutics across the blood-brain barrier. Nat Rev Drug Discov 2021;20(5):362–83.

[31] Donato R. S100: a multigenic family of calcium-modulated proteins of the EF-hand type with intracellular and extracellular functional roles. Int J Biochem Cell Biol 2001;33(7):637–68.

[32] Guo J, Xu B, Han Q, Zhou H, Xia Y, Gong C, et al. Ferroptosis: a novel anti-tumor action for cisplatin. Cancer Res Treat 2018;50(2):445–60.

[33] Tang D, Kang R, Berghe TV, Vandenabeele P, Kroemer G. The molecular machinery of regulated cell death. Cell Res 2019;29(5):347–64.